Multi-mode passive piezoelectric shunt damping by means of matrix inequalities

M. Berardengo [a], S. Manzoni [b,n], A.M. Conti [b]

[a] Università degli Studi di Parma - Department of Engineering and Architecture, Parco Area delle Scienze, 181/A, 43124 Parma, Italy [b] Politecnico di Milano – Department of Mechanical Engineering, Via La Masa, 34, 20156 Milan, Italy

This paper deals with the use of matrix inequalities for the aim of multi-modal piezoelectric shunt damping. The paper shows that the shunt impedance can be seen as a controller in a state space model of the electro-mechanical system; this makes it possible to use the mentioned approach to find the layout of the impedance for different kinds of control problems. The particular focus is on passive multi-mode vibration control with the aim of finding the optimal shunt impedance among the passive and realizable candidates. The proposed method overcomes most of the problems related to the development of the optimal shunt electrical network, which arise when using the most common shunt design strategies for multi-mode control. The results were validated experimentally and compared to well-established methods for multi-mode shunt damping. The proposed method proved to be effective, and the results demonstrate the capability of the matrix inequality approach to provide attenuation levels that are usually higher than those from the reference methods.

Keywords: Piezoelectric shunt, Vibration control, Shunt damping, Multi-mode control, Passive control, Matrix inequality

1. Introduction

The use of piezoelectric actuators shunted to electric impedances as vibration controllers is a well-established topic [1]. According to the kind of impedance used, it is possible to provide a vibrating structure with a control action focused on just one mode or on several modes together. In the former case, the impedances commonly used are a simple resistance [1,2] and the parallel or series connection of a resistance and an inductance [1–5].

There are several possibilities to build the shunt impedance for multi-mode control:

1. the use of a negative capacitance (NC) [6–10] coupled to a resistance. Indeed, the coupling between an NC (which is an active component made from an operational amplifier [11–13]) and a simple resistance can provide a broadband damping action and thus control different modes together [6,9,14]. However, the use of an NC makes the control semi-active and thus poses some problems related to system instability;
2. the use of non-linear shunt impedances based on switches (e.g. [15,16]). Such methods offer good control performance. This approach can sometimes require a complex controller structure when the switches in the shunt impedance have to be driven by digital systems. Nevertheless, Lallart et al. [17] demonstrated that this complexity can be reduced by using self-powered circuits that can remove the need for digital controllers;

Article history:
Received 31 October 2016
Received in revised form 22 May 2017
Accepted 1 June 2017
Handling Editor: A.V. Metrikine

* Corresponding author.
E-mail address: stefano.manzoni@polimi.it (S. Manzoni).

3. the use of passive impedances (i.e. made from resistances, inductances, and capacitances) that are properly designed to tune the control action on the modes considered. This approach does not suffer from any possible problem related to instability thanks to the passive nature of the shunt impedance, and it does not require any digital system or feedback sensor.

The third approach plays an important role due to its passivity, lack of instability, and lack of additional devices, especially in the industrial and aerospace fields. There are different methods of designing a proper shunt impedance for a given control problem. The methods can be divided in to those that work with either one or more piezoelectric actuators, and those based on several piezoelectric actuators together, which often exploit the advantages of periodic structures.

For the first type, Hollkamp was the first to propose an impedance design method using a single piezoelectric patch working on different modes at the same time [18]. The proposed network design is made from as many branches connected in parallel as the number of modes to be damped. The main problems related to this method are the cross-talk between the branches of the circuit, which requires perfectly decoupled modes, and the complexity of the procedure to fix the values of all the electric components.

Wu [19] and Behrens et al. [20] respectively proposed the current blocking (CB) and current flowing (CF) methods, where the shunt impedance is again made from as many branches as the number of modes to control. All the branches are again connected in parallel. In CB [19], there are N_i elements in each branch connected in series (where N_i is the number of modes to be damped). The first of these elements is a parallel connection of a resistance and an inductance, while the other elements are parallel connections of a capacitance and an inductance. Although a method was proposed to simplify the design of the shunt impedance somewhat, the complexity of the circuit is evident, especially when the number of modes to control increases. Another problem with the CB method is that there are some degrees of freedom in the tuning of the network. Indeed, the values of some electric components must be fixed arbitrarily without any guidelines, which results in non-optimal control actions.

In the CF technique [20], each branch is made from three elements: a resistance, a capacitance, and an inductance. The values of the resistances in the shunt impedance must be fixed by numerical minimisation [21]. Furthermore, there are some degrees of freedom that lead to a non-optimal solution in this case as well, although Cigada et al. [22] proposed some guidelines to overcome this problem. There are also cross-talk effects that are not accounted for in the tuning procedure and can be solved just by using numerical minimisations [22].

Fleming et al. [23] introduced a smart method that can be seen as a mix of CB and CF. The shunt network is a combination of cells connected in series and parallel (i.e. series-parallel approach). Like in other approaches [19,20], the main drawback of the method is that there are some degrees of freedom in the tuning of the network with arbitrarily fixed component values. The same paper also shows that adding a capacitor to the shunt circuit decreases the global coupling coefficient and thus the damping performance. This effect is related to all multi-mode shunts working with a single patch because of the unavoidable addition of capacitors in the shunt circuit [24]. This problem could be mitigated by using multiple piezoelectric actuators.

Several techniques have also been proposed to tune the shunt impedances using more than one piezoelectric actuator together. Moheimani et al. [25] proposed a multi-mode control approach with more than one piezoelectric actuator shunted by a multi-input impedance, which relies on the representation of the shunt damping as a feedback controller. They presented only tests carried out with a synthetic controller. The method provides good performance, but there are again some degrees of freedom that must be fixed by the user without any guidelines. Moreover, Fleming and Moheimani [26] presented an approach to design shunt impedances for multi-mode control based on well-established methods such as linear quadratic Gaussian (LQG) control, H_2 control, and H_∞ control. This approach works with one or more piezoelectric actuators. The three control methods were compared, showing that shunts can provide good attenuation performance. However, the main issue is that LQG and H_∞ controllers required active components in the shunt impedance (e.g. negative reactive components).

Maurini et al. [27] studied electric vibration absorbers made of distributed piezoelectric devices for the control of beam vibrations. The absorbers were obtained by interconnecting an array of piezoelectric transducers uniformly distributed on a beam with different modular electric networks. The electrical network is expected to show resonances at specific target frequencies. Batra et al. [28] showed that this is possible by interconnecting passive branches comprising inductances and capacitances. Giorgio et al. [29] proposed a method to control N_i modes of undamped systems with N_i interconnected actuators. The approach does not guarantee the realisation of the network with passive elements, even if further complication of the method could allow this constraint to be satisfied. Andreaus et al. [30] proposed a method for controlling the flexural vibrations of beams with more than one actuator by finding an electrical circuit analogue to a Timoshenko beam through a Lagrangian method. The main limit of this approach is related to the lumped nature of the piezoelectric devices used and the electric circuit, which link the lowest controllable wavelength to the size of the piezoelectric patch (i.e. the lowest controllable wavelength is approximately equal to the size of the actuators). However, the problem can be limited by using enough elements per wavelength. Moreover, given the electrical network, the values of the capacitive and inductive elements are fixed to match the mechanical resonances of the beam. As for the resistances, the tuning procedure is not straightforward. Although some approaches to tune additional resistances are given to provide the appropriate damping to the electric impedance, no criteria are available to fulfil a given control problem (e.g. H_∞). Bisegna et al. [31] proposed a multi-modal vibration damping method for an elastic beam equipped with multiple piezoelectric actuators connected to an

electric network. Two analytical models of the electromechanical coupled structure were considered: a homogenized one and a discrete one. Lossouarn et al. [32] recently proposed a multi-modal control strategy by coupling a beam to a network representing its electrical analogue. Such a network is designed by using the direct electromechanical analogy applied to a transverse lattice of point masses representing the discrete model of the beam. The electrical and mechanical structures are then linked by an array of piezoelectric actuators. The main drawback of the approach, which is currently under investigation, is again that no clear criteria are available for fixing the properties of the additional resistances to be added to the shunt network for tuning the damping levels. The extension to bi-dimensional structures (e.g. plates) of the methods based on shunt networks that are the electrical equivalent of the mechanical system would require the synthesis of a lumped circuit analogue to a Kirchhoff-Love plate discretised by the finite difference method. This would significantly increase the problem complexity in terms of both the procedure to derive the shunt network and the network layout. Lossouarn et al. [33] recently addressed this problem and proposed a new method to derive the electrical analogue of a bi-dimensional structure. The method relies on a finite difference approximation of the Kirchhoff–Love theory and the use of the direct electromechanical analogy.

To improve the performance of the traditional techniques used with a single piezoelectric actuator, Airoldi and Ruzzene [34] showed that CB coupled to a periodic layout of piezoelectric actuators can improve much of the attenuation performance provided by the pure CB, thanks to the bandgaps generated by periodicity.

Collet et al. [35] developed a numerical method for modelling and optimising two-dimensional smart metacomposites (i.e. distributed shunted piezoelectric patches). This numerical technique was proved to be capable of coping with the multimodal wave dispersion behaviour over the whole first Brillouin zone when considering periodically distributed two-dimensional shunted piezomechanical systems.

Bao et al. [36] and Yan et al. [37] recently developed multi-modal attenuation methods by means of non-linear shunted piezoelectric actuators for periodic structures. Such an approach exploits non-linear switching shunt impedances in the context of periodic structures with good results.

Despite all the described tuning strategies offering good results, the main limitation is that they refer to specific applications, such as the control of beams or plates or the use of one or more actuators. Furthermore, they often do not allow for a specific control target to be set. Thus, this paper presents a new general approach to multi-mode vibration reduction that can be applied to both mono- and bi-dimensional structures by employing either one or more piezoelectric actuators. Therefore, the method does not necessarily rely on distributed structure layouts. Moreover, the proposed approach is aimed at providing the optimal controller for given control applications, and it relies on the linear matrix inequality (LMI) theory. The LMI approach allows for a control target to be set (e.g. H_2 or H_∞ on displacement, velocity, or acceleration) and for constraints to be imposed on the control features. The particular focus is on passive control. Therefore, the method allows an expression of the shunt impedance to be found that satisfies the fixed control target, assuring that it can be realised by a passive physical network.

The layout of the paper is as follows. Section 2 presents the model used to describe the electro-mechanical structure. Section 3 explains how to apply the LMI approach to piezoelectric shunt and how to set and solve the control problem by even imposing passivity and conditions to make the electric network feasible. Section 4 explains how to derive the shunt impedance layout. Finally, Section 5 shows the experiments carried out to demonstrate the reliability of the approach.

2. System model

The model of the electro-mechanical system (EMS, composed of the vibrating structure, the piezoelectric actuator, and the shunt impedance) must describe both the mechanical and the electrical dynamics. We consider a generic structure excited by an external forcing $\mathbf{F}_{\text{ext}}$, where the actuator is shunted by an impedance Z (see Fig. 1a). Q_p is the charge in the upper electrode ($-Q_\text{p}$ in the lower electrode), and V_p is the voltage between the electrodes. The displacement W of any point x of the structure at time t can be expressed as a modal summation:

$$W(x,t) = \sum_{r=1}^{N} \Phi_r(x) q_r(t) \tag{1}$$

where q_r is the r^{th} modal coordinate, N is the number of modes considered (theoretically $N \to \infty$), and Φ_r is the r^{th} eigenmode (scaled to the unit modal mass) of the structure. The modal coordinates are the solutions of the following problem [2,6,38,39]:

$$\ddot{q}_r + 2\xi_r\omega_r\dot{q}_r + \omega_r^2 q_r - \chi_r V_\text{p} = F_r \quad \forall\, r\epsilon\{1,\ldots,N\} \tag{2}$$

$$C_\infty V_\text{p} - Q_p + \sum_{l=1}^{N} \chi_l q_l + \frac{\int V_\text{p}}{R_\text{p}} = 0 \tag{3}$$

where ω_r is the r^{th} eigenfrequency of the EMS in short-circuit (SC, i.e. $Z = 0$), ξ_r is the associated non-dimensional damping ratio, and F_r is the harmonic modal force. χ_r is a modal coupling coefficient that describes the energy transfer

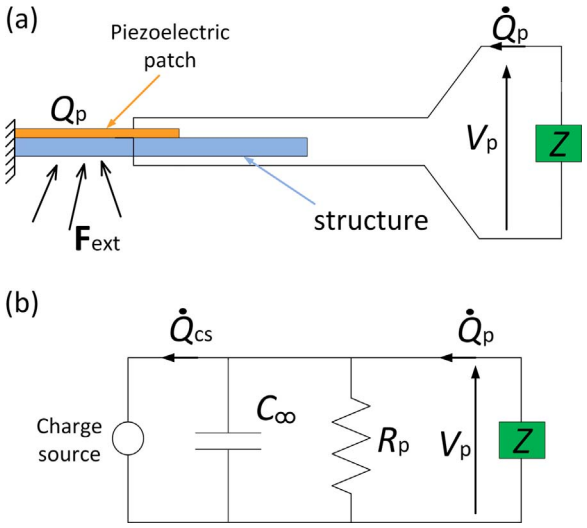

Fig. 1. A generic structure with a shunted piezoelectric patch (a) and electric model of the EMS (b).

between the piezoelectric patch and the r^{th} mode. Thus, the behaviour of the EMS is described by two equations: Eq. (2) and Eq. (3). Eq. (2) describes the equations of motion of the system. The term χ_r couples these equations of motion to Eq. (3), which models the electric behaviour of the EMS (see Fig. 1b, where the term $\sum_{l=1}^{N}\chi_l\dot{q}_l$ is abbreviated as $\dot{Q}_{cs}$). C_∞ is the electrical capacitance of the piezoelectric patch with blocked structure, which also corresponds to the value of the capacitance at infinite frequency [6]. R_p is the resistance associated with the piezoelectric patch, which is usually very high [40]. $\int V_p$ is intended as an integral in time (i.e. $\int V_p dt$).

The terms χ_r can be found analytically [39], through a finite element model [38], or experimentally by measuring the effective coupling coefficients associated with each mode [6] (see Section 5.1). In the case of low modal density, if we consider only the modes between the u^{th} (i.e. $r = u$) and the h^{th} modes (i.e. $r = h$, with $h > u$), Eqs. (2) and (3) can be written as:

$$\ddot{q}_r + 2\xi_r\omega_r\dot{q}_r + \omega_r^2 q_r - \chi_r V_p = F_r \quad \forall\, r\epsilon\{u,\ldots,h\} \tag{4}$$

$$C_\infty V_p - Q_p + \sum_{l=u}^{h}\chi_l q_l + \frac{\int V_p}{R_p} + SV_p + MV_p = 0 \tag{5}$$

where S is a term that accounts for the contribution of the modes lower than the u^{th} mode, while M is a term that accounts for the contribution of the modes higher than the h^{th} mode. According to previous studies [6,9], we have:

$$S = 0 \text{ and } M = \sum_{n=h+1}^{N}\frac{\chi_n^2}{\omega_n^2} \tag{6}$$

Therefore, Eq. (5) can be rearranged as:

$$C_p V_p - Q_p + \sum_{l=u}^{h}\chi_l q_l + \frac{\int V_p}{R_p} = 0 \tag{7}$$

where:

$$C_p = C_\infty + \sum_{n=h+1}^{N}\frac{\chi_n^2}{\omega_n^2} \tag{8}$$

C_p can be found by measuring the value of the capacitance of the piezoelectric actuator midway between ω_h and ω_{h+1} [6]. Hence, the whole dynamics of the EMS in the frequency range of interest is described by Eqs. (4) and (7). To use the LMI approach to solve a given control problem, the EMS model needs to be represented in terms of state space variables. The state space representation provided in this paper plays a key role since it also allows the shunt impedance to be seen as a controller. Indeed, expressing Z as a controller allows the passivity requirement to be imposed directly on the impedance Z in the LMI problem (see Section 3.1.3), which is one of the targets of the proposed control approach. The following subsection explains how to derive the state space representation of the EMS model described by Eqs. (4), (7), and (8).

2.1. State space representation of the electro-mechanical system

According to Eqs. (4) and (7), we can write the following system of equations:

$$\begin{cases} \ddot{q}_r + 2\xi_r\omega_r\dot{q}_r + \omega_r^2 q_r - \chi_r V_\mathrm{p} = F_r \quad \forall\, r\epsilon\{u,\dots,h\} \\ \dot{q}_r = \dot{q}_r \quad \forall\, r\epsilon\{u,\dots,h\} \\ C_\mathrm{p}V_\mathrm{p} - Q_\mathrm{p} + \sum_{l=u}^{h}\chi_l q_l + \frac{\int V_\mathrm{p}}{R_\mathrm{p}} = 0 \end{cases} \tag{9}$$

By defining:

$$\bar{V} = V_\mathrm{p}\sqrt{C_\mathrm{p}} \text{ and } \bar{Q} = \frac{Q_\mathrm{p}}{\sqrt{C_\mathrm{p}}} \tag{10}$$

Eq. (9) can be written as:

$$\begin{cases} \ddot{q}_r + 2\xi_r\omega_r\dot{q}_r + \omega_r^2\left(1+b_r^2\right)q_r + b_r\omega_r\sum_{l=u}^{r-1} b_l\omega_l q_l + b_r\omega_r\sum_{l=r+1}^{h} b_l\omega_l q_l + \frac{b_r\omega_r}{R_\mathrm{p}C_\mathrm{p}}\int\bar{V} = F_r + b_r\omega_r\bar{Q} \quad \forall\, r\epsilon\{u,\dots,h\} \\ \dot{q}_r = \dot{q}_r \quad \forall\, r\epsilon\{u,\dots,h\} \\ \bar{V} = -\sum_{l=u}^{h} b_l\omega_l q_l - \frac{\int\bar{V}}{R_\mathrm{p}C_\mathrm{p}} + \bar{Q} \end{cases} \tag{11}$$

where $b_l = \chi_l/(\omega_l\sqrt{C_\mathrm{p}})$, and $\int\bar{V}$ is intended as an integral in time (i.e. $\int\bar{V}\mathrm{d}t$). The vector $\mathbf{g}$ of the state variables is now defined as:

$$\mathbf{g} = \begin{bmatrix} \dot{q}_u \\ q_u \\ \vdots \\ \dot{q}_h \\ q_h \\ \int\bar{V} \end{bmatrix} \tag{12}$$

The length of vector $\mathbf{g}$ is $2(h-u+1)+1 = n_\mathrm{s}$, where n_s is the order of the system. The system described by Eq. (11) can be written in state space notation:

$$\begin{cases} \dot{\mathbf{g}} = \mathbf{A}\mathbf{g} + \mathbf{B}_\mathrm{w}\bar{Q} + \mathbf{B}_\mathrm{f}\mathbf{F}_\mathrm{ext} \\ z_\mathrm{o} = \mathbf{C}_z\mathbf{g} + \mathbf{D}_\mathrm{zw}\bar{Q} + \mathbf{D}_\mathrm{zf}\mathbf{F}_\mathrm{ext} \\ y = \mathbf{C}_y\mathbf{g} + \mathbf{D}_\mathrm{yw}\bar{Q} + \mathbf{D}_\mathrm{yf}\mathbf{F}_\mathrm{ext} \end{cases} \tag{13}$$

where z_o is the target variable of the control (e.g. the displacement W, velocity $\dot{W}$, and acceleration $\ddot{W}$ of the system computed at a given point x_m of the structure); y is the output of the system, which is $-\int\bar{V}$ in this case. Finally, $\bar{Q}$ is seen as a control action provided to the vibrating system.

If we choose the displacement at a point x_m as the target variable, we have $z_\mathrm{o} = W$. In the case of a single force F_ext acting on point x_f, the matrices of Eq. (13) are:

$$\mathbf{A} = \begin{bmatrix} -2\xi_u\omega_u & -\omega_u^2\left(1+b_u^2\right) & 0 & -\omega_u b_u\omega_{u+1}b_{u+1} & \cdots & 0 & -\omega_u b_u\omega_h b_h & -\frac{b_u\omega_u}{R_\mathrm{p}C_\mathrm{p}} \\ 1 & 0 & 0 & 0 & \cdots & 0 & 0 & 0 \\ 0 & -\omega_{u+1}b_{u+1}\omega_u b_u & -2\xi_{u+1}\omega_{u+1} & -\omega_{u+1}^2\left(1+b_{u+1}^2\right) & \cdots & 0 & -\omega_{u+1}b_{u+1}\omega_h b_h & -\frac{b_{u+1}\omega_{u+1}}{R_\mathrm{p}C_\mathrm{p}} \\ 0 & 0 & 1 & 0 & \cdots & 0 & 0 & 0 \\ \vdots & \vdots & \vdots & \vdots & \vdots & \vdots & \vdots & \vdots \\ 0 & -\omega_h b_h\omega_u b_u & 0 & -\omega_h b_h\omega_{u+1}b_{u+1} & \cdots & -2\xi_h\omega_h & -\omega_h^2\left(1+b_h^2\right) & -\frac{b_h\omega_h}{R_\mathrm{p}C_\mathrm{p}} \\ 0 & 0 & 0 & 0 & \cdots & 1 & 0 & 0 \\ 0 & -\omega_u b_u & 0 & -\omega_{u+1}b_{u+1} & \cdots & 0 & -\omega_h b_h & -\frac{1}{R_\mathrm{p}C_\mathrm{p}} \end{bmatrix} \tag{14}$$

$$\mathbf{B}_{\mathrm{f}} = \begin{bmatrix} \Phi_u(x_f) \\ 0 \\ \Phi_{u+1}(x_f) \\ 0 \\ \vdots \\ \Phi_h(x_f) \\ 0 \\ 0 \end{bmatrix} \quad \mathbf{B}_{\mathrm{w}} = \begin{bmatrix} \omega_u b_u \\ 0 \\ \omega_{u+1} b_{u+1} \\ 0 \\ \vdots \\ \omega_h b_h \\ 0 \\ 1 \end{bmatrix} \tag{15}$$

$$\mathbf{C}_{\mathrm{z}} = \begin{bmatrix} 0 & \Phi_u(x_{\mathrm{m}}) & 0 & \Phi_{u+1}(x_{\mathrm{m}}) & \cdots & 0 & \Phi_h(x_{\mathrm{m}}) & 0 \end{bmatrix}, \mathbf{C}_{\mathrm{y}} = \begin{bmatrix} 0 & \cdots & 0 & -1 \end{bmatrix}, \mathbf{D}_{\mathrm{zw}} = \mathbf{D}_{\mathrm{zf}} = \mathbf{D}_{\mathrm{yw}} = \mathbf{D}_{\mathrm{yf}} = 0 \tag{16}$$

The size of the matrix $\mathbf{A}$ is $[2(h-u+1)+1]\mathrm{x}[2(h-u+1)+1]$, while the length of vectors $\mathbf{B}_{\mathrm{f}}$, $\mathbf{B}_{\mathrm{w}}$, $\mathbf{C}_{\mathrm{y}}$, and $\mathbf{C}_{\mathrm{z}}$ is $2(h-u+1)+1$.

It is noticed that the model can be easily extended to the case of more than one disturbance force acting on the system. Moreover, Appendix A gives the expression of the matrices of the state space system for the cases of $z_{\mathrm{o}} = \dot{W}$ and $z_{\mathrm{o}} = \ddot{W}$.

The model can be easily extended to the case where two or more piezoelectric patches are connected in series/parallel, as well as the case of an NC connected to the patch. Indeed, in both cases, Eq. (9) is still valid, provided that new system parameters are used:

- in the case of a series/parallel connection of piezoelectric actuators, we have an equivalent piezoelectric actuator. The values of the equivalent χ_r, C_{p}, and ω_r due to all the actuators must be calculated or measured for the new equivalent EMS [38];
- in the case of an NC connected to the piezoelectric actuators, the equivalent C_{p} value (and ω_r in the case of a series connection between the patch and the NC) due to the addition of the NC must be calculated or measured for the new equivalent EMS [6].

Therefore, the state space representation described by Eq. (13) is generally valid.

The state space model describes the EMS as a controlled system via a feedback loop, as illustrated in Fig. 2 (where $\mathbf{D}_{\mathrm{yw}}$ and $\mathbf{D}_{\mathrm{yf}}$ are not shown because they are always null matrices). This is accomplished by considering $\bar{Q}$ as a control action and $-\int\bar{V}$ as the output of the system. Based on Fig. 1b and Eq. (10), the transfer function of the controller K (see Fig. 2) can be expressed as:

$$K = \frac{\bar{Q}}{-\int\bar{V}} = \frac{\dot{Q}_{\mathrm{p}}}{-C_{\mathrm{p}}V_{\mathrm{p}}} = \frac{1}{C_{\mathrm{p}}Z} = \frac{Y}{C_{\mathrm{p}}} \tag{17}$$

where the admittance Y is $1/Z$. Hence, the model presented herein can describe the EMS as a system controlled by a feedback loop, and the controller is the electric admittance shunted to the piezoelectric actuator (divided by C_{p}). This control problem is an output feedback problem.

It is now possible to set the control targets and the constraints on the controller structure. The next section discusses how to translate these requirements to an LMI problem and how to find the most suitable transfer function of Z.

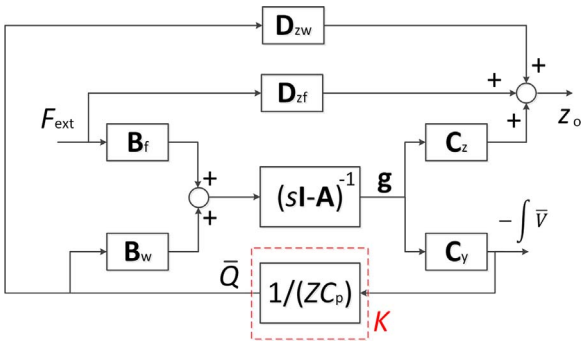

Fig. 2. Output feedback scheme in the Laplace domain, where s is the Laplace operator and $\mathbf{I}$ is the identity matrix.

3. The use of linear matrix inequalities in piezoelectric shunt damping

In the controller synthesis process, the main goal is to design a controller with characteristics that satisfy a given target, which is multimodal control in this case. Moreover, constraints on the controller characteristics may sometimes be required as well, and the passivity of the shunt network is addressed in this paper. The main drawback of the passive shunt damping is that the achievable performance is strongly dependent on very fine tuning of the whole control system. For this reason, much effort must be spent in the process of controller optimisation to achieve satisfactory vibration attenuation performance.

In this scenario, the definition of a design approach for the controller that can simultaneously account for the control target and the passivity constraint of the network is fundamental. As mentioned in Section 1, the most common approach is based on the choice of the passive network layout (i.e. a positive real function), which has a fixed layout. Its parameters are then optimised to minimise the given objective function. The most relevant methods that rely on this approach are the CB and the CF techniques [19,20]. However, one of the drawbacks related to these techniques is that the choice of the optimal controller is limited by its fixed structure. Therefore, not all possible passive network layouts are considered in the optimisation process. It follows that the structure of the electrical network is not optimised, and therefore, the approach might not lead to the optimal network among all the possible configurations, thus limiting the performance of the control as well.

In light of this, we focused our attention on the LMI approach, which allows for the control targets ranging over all the possible passive networks to be satisfied. Indeed, the LMI approach allows the synthesis of the optimal admittance Y over the class of all the positive real functions that guarantee the physical feasibility of the network. It uses a state space representation of the system and the classical approach for controller synthesis. Since the admittance Y (as well as the impedance Z; see Eq. (17)) is seen as a controller in the state space representation of the EMS (see Section 2.1), the search for passive impedances translates to a search for passive controllers.

The LMI approach is emerging as a powerful tool to solve control problems, especially thanks to the possibility of managing different kinds of targets. Several objective functions can be expressed as LMIs, such as the H_2 norm, which can be used to impose limits on signal root mean square (RMS), the H_∞ norm to limit the frequency response function (FRF) peak, pole placement, robust regulation, as well as the passivity of the controller. Moreover, even multi-objective control can be addressed with the LMI approach [41–44] by considering two or more objective functions in the optimisation problem.

This work focuses on single- and multi-objective optimisation problems involving the passivity constraint of the shunt impedance (i.e. the controller) and the H_2 and H_∞ norms as objective functions. Nevertheless, the procedure showed in the following can be easily extended to any kind of control target that can be expressed as a matrix inequality. Section 3.1 shows the LMI formulation for the two control targets considered (H_2 and H_∞) and for the passivity constraint. The mentioned section deals with single-objective optimisation, and therefore each control problem is presented separately. Section 3.2 addresses the matrix inequality formulation for multi-objective control.

3.1. LMI formulation of the objective functions

In this section, the H_2 and H_∞ control as well as the passivity of the controller are formulated as LMI problems. Control specifications for the closed-loop transfer function T_{zF} linking the disturbance F_{ext} and the target variable of the control z_o are taken into account. Referring to Fig. 2, T_{zF} can be expressed in the Laplace domain as:

$$T_{zF} = \mathbf{C}_z(s\mathbf{I}-[\mathbf{A} + \mathbf{B}_w K \mathbf{C}_y])^{-1}\mathbf{B}_f + \mathbf{D}_{zw} K \mathbf{C}_y(s\mathbf{I}-[\mathbf{A} + \mathbf{B}_w K \mathbf{C}_y])^{-1}\mathbf{B}_f + \mathbf{D}_{zf} \tag{18}$$

where s is the Laplace operator, and $\mathbf{I}$ is the identity matrix. All the matrices that are always null (i.e. regardless of whether the target variable is displacement, velocity, or acceleration) are neglected in Eq. (18).

A state space representation of the controller K can be derived as well:

$$\begin{cases} \dot{\mathbf{g}}_\mathbf{k} = \mathbf{A}_k \mathbf{g}_k + \mathbf{B}_k y \\ \bar{Q} = \mathbf{C}_k \mathbf{g}_k + \mathbf{D}_k y \end{cases} \tag{19}$$

where $\mathbf{A}_k$, $\mathbf{B}_k$, $\mathbf{C}_k$, and $\mathbf{D}_k$ are the state space matrices of the controller, and $\mathbf{g}_k$ is the state vector. The transfer function of the controller K can thus be expressed as:

$$K(s) = \mathbf{C}_k(s\mathbf{I} - \mathbf{A}_k)^{-1}\mathbf{B}_k + \mathbf{D}_k \tag{20}$$

The state space representation of the closed-loop system is then obtained from Eqs. (13) and (19):

$$\begin{cases} \dot{\mathbf{g}}_{cl} = \mathbf{A}_{cl}\mathbf{g}_{cl} + \mathbf{B}_{cl}F_{ext} \\ z_o = \mathbf{C}_{cl}\mathbf{g}_{cl} + \mathbf{D}_{cl}F_{ext} \end{cases} \tag{21}$$

where the closed-loop state vector is:

$$\mathbf{g}_{cl} = \begin{bmatrix} \mathbf{g} \\ \mathbf{g}_k \end{bmatrix} \tag{22}$$

The expressions of matrices $\mathbf{A}_{cl}$, $\mathbf{B}_{cl}$, $\mathbf{C}_{cl}$, and $\mathbf{D}_{cl}$ are provided in Appendix B. Hence, the transfer function T_{zF} of Eq. (18) can be expressed as a function of the closed-loop matrices using Eq. (21):

$$T_{zF} = \mathbf{C}_{cl}(s\mathbf{I} - \mathbf{A}_{cl})^{-1}\mathbf{B}_{cl} + \mathbf{D}_{cl} \tag{23}$$

In the LMI approach, each control target or specification is expressed as a constraint on the admissible Lyapunov functions for the internally stable closed-loop system [43]:

$$\exists\ V(\mathbf{g}_{cl}) = \mathbf{g}_{cl}^{T}\mathbf{P}\mathbf{g}_{cl},\ \mathbf{P} > 0 : \mathbf{A}_{cl}^{T}\mathbf{P} + \mathbf{P}\mathbf{A}_{cl} < 0 \tag{24}$$

where V is a quadratic Lyapunov function, $\mathbf{P}$ is the Lyapunov matrix, $\mathbf{g}_{cl}$ is the closed-loop state-space vector, and $\mathbf{A}_{cl}$ is the state matrix of the system. The superscript T indicates the transposed matrix.

Since the additional constraints are related to targets on the transfer function T_{zF} of Eq. (23), the related LMI formulation will be thus expressed as a function of the closed-loop matrices $\mathbf{A}_{cl}$, $\mathbf{B}_{cl}$, $\mathbf{C}_{cl}$, and $\mathbf{D}_{cl}$ (see Eqs. (25) and (26) further in the paper). Therefore, the solution of the LMI problem will provide state space matrices that satisfy the given specifications. Then, according to the expressions in Appendix B, the matrices $\mathbf{A}_k$, $\mathbf{B}_k$, $\mathbf{C}_k$, and $\mathbf{D}_k$ of the controller and the transfer function K can be derived. Subsections 3.1.1 to 3.1.3 show the LMI constraints related to the different control specifications addressed in the paper (H_∞ control, H_2 control, and passivity, respectively).

3.1.1. H_∞ control

For H_∞ control, the objective is to find a controller K such that $\|T_{zF}\|_\infty$ is minimised. As demonstrated in [42,43] , there exists a controller K such that $\|T_{zF}\|_\infty < \gamma$ and $\mathbf{A}_{cl}$ is stable if and only if the following problem is feasible for some symmetric $\mathbf{P}>0$, $\gamma > 0$, and $\mathbf{A}_k$, $\mathbf{B}_k$, $\mathbf{C}_k$, and $\mathbf{D}_k$ of compatible dimensions [45]:

$$\begin{bmatrix} \mathbf{A}_{cl}^{T}\mathbf{P} + \mathbf{P}\mathbf{A}_{cl} & \mathbf{P}\mathbf{B}_{cl} & \mathbf{C}_{cl}^{T} \\ \mathbf{B}_{cl}^{T}\mathbf{P} & -\gamma\mathbf{I} & \mathbf{D}_{cl}^{T} \\ \mathbf{C}_{cl} & \mathbf{D}_{cl} & -\gamma\mathbf{I} \end{bmatrix} < 0 \tag{25}$$

It follows that the solution of the problem requires minimising γ.

3.1.2. H_2 control

In this case, the control target is to design a controller K such that $\|T_{zF}\|_2$ is minimised. As can be demonstrated [43], there exists a controller K such that $\|T_{zF}\|_2 < \mu$ and $\mathbf{A}_{cl}$ is stable if and only if the following problem is feasible for some symmetric $\mathbf{P}>0$, $\mathbf{Q}$, μ^2, and $\mathbf{A}_k$, $\mathbf{B}_k$, $\mathbf{C}_k$, and $\mathbf{D}_k$ of compatible dimensions [43]:

$$\begin{bmatrix} \mathbf{A}_{cl}^{T}\mathbf{P} + \mathbf{P}\mathbf{A}_{cl} & \mathbf{P}\mathbf{B}_{cl} \\ \mathbf{B}_{cl}^{T}\mathbf{P} & -\mathbf{I} \end{bmatrix} < 0, \begin{bmatrix} \mathbf{P} & \mathbf{C}_{cl}^{T} \\ \mathbf{C}_{cl} & \mathbf{Q} \end{bmatrix} > 0,\ \mathrm{tr}(\mathbf{Q}) < \mu^2,\ \mathbf{D}_{cl} = \mathbf{0} \tag{26}$$

where $\mathbf{Q}$ is a symmetric matrix. It can be deduced from Eq. (26) that the solution to the problem requires minimising μ.

It is noticed that, according to Appendices A and B, the condition $\mathbf{D}_{cl} = \mathbf{0}$ is never fulfilled when controlling acceleration (i.e. $z_o = \ddot{W}$). Therefore, the present problem formulation prevents the control of acceleration when the target is to minimise H_2 norm. Conversely, H_∞ control can be carried out when $z_o = \ddot{W}$ because the condition $\mathbf{D}_{cl} = \mathbf{0}$ is not required (see Section 3.1.1, Eq. (25)).

3.1.3. Passivity

The passivity of the controller represents an additional constraint in the minimisation problem, and it can be expressed as an LMI as well. In this case, the unknown variables are the controller matrices $\mathbf{A}_k$, $\mathbf{B}_k$, $\mathbf{C}_k$, and $\mathbf{D}_k$. The passivity of the controller can be expressed as a quadratic function:

$$\int_{-\infty}^{t_x} -\dot{Q}_p(t)V_p(t)\mathrm{d}t \geq 0,\ \forall\ \dot{Q}_p(t),\ V_p(t) \tag{27}$$

where t_x is the integration time, $\dot{Q}_p$ is the current flowing in the controller, and V_p is the voltage at its terminals. If passivity is satisfied, then the transfer function of the controller is positive real. Therefore, the passivity of the controller can be expressed as an LMI constraint using the positive real lemma [42]. It follows that a controller $K(s)$ is positive real if and only if there exists $\mathbf{P}>0$ such that:

$$\begin{bmatrix} \mathbf{A}_k^T\mathbf{P} + \mathbf{P}\mathbf{A}_k & \mathbf{P}\mathbf{B}_k - \mathbf{C}_k^T \\ \mathbf{B}_k^T\mathbf{P} - \mathbf{C}_k & -\mathbf{D}_k^T - \mathbf{D}_k \end{bmatrix} \leq 0 \tag{28}$$

where $\mathbf{P}$ is the Lyapunov matrix.

According to Eq. (17), the passivity of the controller implies the passivity of the impedance Z. Eqs. (25), (26), and (28) show how it is possible to translate the target of the control problem and the constraints on the controller features into LMIs. Nevertheless, the careful reader could easily notice that, actually, Eqs. (25), (26), and (28) do not represent LMIs since the dependence on the decision variables is not linear. As an example, referring to Eq. (25), the expression $\mathbf{A}_{cl}^T\mathbf{P} + \mathbf{P}\mathbf{A}_{cl}$ is not affine in the variables $\mathbf{P}$ and $\mathbf{A}_{cl}$. Indeed, it involves the product between the controller variables (which are included in the $\mathbf{A}_{cl}$ expression, see Appendix B) and the Lyapunov matrix $\mathbf{P}$. Consequently, these problems are non-linear and thus cannot be solved by LMI optimisation (e.g. using the ellipsoid method or the interior-point method [44,46]). Nevertheless, for the state feedback case and even for the output feedback systems (which is the case considered in this paper), there exists a change of variables that makes all the inequalities affine in a new set of unknowns, thus making the constraints linear and easily solvable [43].

3.2. Multi-objective control

In the case of multi-objective control, two or more specifications must be addressed at the same time. Therefore, the goal of the optimisation process is to derive a stabilising controller K that allows for all targets to be satisfied at the same time. As an example, the case of mixed H_2 / H_∞ control is presented.

In this problem, the target is to minimise the norm $\|T_{zF}\|_2$ while taking into account a constraint on the value of $\|T_{zF}\|_\infty$, which is fixed. Therefore, as soon as the limit on the H_∞ norm γ is assigned, there exists a controller K such that $\|T_{zF}\|_2 < \mu$, $\|T_{zF}\|_\infty < \gamma$, and $\mathbf{A}_{cl}$ is stable if and only if the following problem is feasible for some $\mathbf{P}_\infty > 0, \mathbf{P}_2 > 0$, $\mathbf{Q}$, μ^2, and $\mathbf{A}_k$, $\mathbf{B}_k$, $\mathbf{C}_k$, and $\mathbf{D}_k$ of compatible dimensions [42]:

$$\begin{bmatrix} \mathbf{A}_{cl}^T\mathbf{P}_2 + \mathbf{P}_2\mathbf{A}_{cl} & \mathbf{P}_2\mathbf{B}_{cl} \\ \mathbf{B}_{cl}^T\mathbf{P}_2 & -\mathbf{I} \end{bmatrix} < 0, \quad \begin{bmatrix} \mathbf{P}_2 & \mathbf{C}_{cl}^T \\ \mathbf{C}_{cl} & \mathbf{Q} \end{bmatrix} > 0, \quad \mathrm{tr}(\mathbf{Q}) < \mu^2, \quad \mathbf{D}_{cl} = \mathbf{0},$$
$$\begin{bmatrix} \mathbf{A}_{cl}^T\mathbf{P}_\infty + \mathbf{P}_\infty\mathbf{A}_{cl} & \mathbf{P}_\infty\mathbf{B}_{cl} & \mathbf{C}_{cl}^T \\ \mathbf{B}_{cl}^T\mathbf{P}_\infty & -\gamma\mathbf{I} & \mathbf{D}_{cl}^T \\ \mathbf{C}_{cl} & \mathbf{D}_{cl} & -\gamma\mathbf{I} \end{bmatrix} < 0 \tag{29}$$

where $\mathbf{P}_\infty$ is the Lyapunov matrix related to the H_∞ problem, while $\mathbf{P}_2$ is the Lyapunov matrix related to the H_2 problem. The subscripts of the Lyapunov matrices are indeed used to mark and discriminate the Lyapunov matrices related to the two different control problems (H_∞ and H_2 in this example).

The first set of inequalities is related to the H_2 specification (see Eq. (26)), while the second is related to the constraint on the H_∞ norm (see Eq. (25)). This kind of problem will provide a solution that is a trade-off between the results of the H_∞ and H_2 solutions.

All the inequalities of Eq. (29) must be satisfied at the same time by the single feedback gain K, and thus the problem is non-convex in the variables $\mathbf{P}_2$, $\mathbf{P}_\infty$, $\mathbf{A}_k$, $\mathbf{B}_k$, $\mathbf{C}_k$, $\mathbf{D}_k$, μ, and $\mathbf{Q}$. To treat the problem in the LMI framework, it is necessary to look for a single Lyapunov matrix:

$$\mathbf{P} = \mathbf{P}_2 = \mathbf{P}_\infty \tag{30}$$

and then to introduce a change of the controller variables [43] that makes all the inequalities affine in the problem variables, as already mentioned for the single-objective control.

As shown in the example related to mixed H_2/H_∞ control, all the types of constraints expressed as matrix inequalities can be combined to set the desired multi-objective problem. Such problems lead to a set of nonlinear matrix inequalities that cannot be solved with the LMI approach.

To face this problem, as already mentioned, some linearization procedures can be applied to the output feedback systems [43], allowing for a solution of the original set of nonlinear inequalities. Nevertheless, despite this linearization represents a solution to the multi-objective output feedback control, it introduces some conservatism and therefore suffers from some limitations. First of all, the change of the controller variables, proposed in [43] to linearize the matrix inequalities, requires the order of the controller n_k to be equal to that of the system (i.e. $n_k = n_s$). This translates to the restriction of the possible controllers considered for solving the control problem. Secondly, the constraint of Eq. (30) must be added to address multi-objective problems. This introduces conservatism in the solution, imposing a common Lyapunov matrix as a solution of all sets of matrix inequalities (one set for each control objective/specification). Finally, the linearization process can lead to an ill-conditioned problem, especially if added states are present in the state-space representation of the considered systems

[45] (such as the integral of the voltage in the case considered). It is remarked that, despite its effectiveness in solving the problem, such a linearization is not straightforward. Although there are methods to apply linearization even when reduced-order controllers are searched for (as in the present application), the complexity of these methods increases substantially, and their application is thus difficult [43]. For these reasons, we approach the nonlinear problem in two different ways: the linearization of the problem using approximations and the use of non-linear solvers. The two solutions are described and discussed in Section 3.3.

3.3. The solution of bilinear matrix inequalities

As mentioned in the previous section, the multi-objective output feedback control problem leads to a non-linear matrix inequality problem — in particular, a bilinear matrix inequality (BMI) problem. The control problem has been formulated as a BMI to overcome the limitations introduced by the linearization and to propose an optimisation that allows for any order of the controller. Two procedures for the solution of the non-linear problem were applied. The first is an iterative procedure based on the linearization of the problem using approximations, which allows for the BMI to be solved locally and enables the use of linear solvers (see Section 3.3.1). The second is using non-linear solvers (see Section 3.3.2).

3.3.1. Iterative solution of the BMI

The use of linear solvers (e.g. based on the interior-point approach) requires linearizing the BMI using approximations to obtain an LMI problem again. One of the main drawbacks of this approach is that a local solution (local minimum) can be found, meaning there is no assurance of finding the optimal solution. Different linearization methods are available, such as an iterative procedure proposed in [45] and the path following algorithm [47].

This approach showed to be very sensitive to numerical problems. One reason is that the problem variables stretch over wide ranges (e.g. on order of 10^6 for $\mathbf{P}$ and the order of 10^{-6} for γ and μ). Another is the presence of sparse matrices. We tested this approach using solvers based on the interior point algorithm [46] and managed them with YALMIP [48,49]. They provided good results when only one structural mode had to be damped, but failure often occurred when increasing the number of modes to be controlled. Actually, only one of the solvers tested (MOSEK [50]) sometimes provided satisfactory results, even when increasing the number of modes.

3.3.2. Non-linear solvers

The use of non-linear solvers based on the Newton method [51] or the trust region method [52] were much more reliable. The trust region method is more robust than the Newton method when sparse matrices must be managed [51], as in this case, so we decided to focus on this algorithm. The results achieved were much more reliable than when using the iterative approach based on linearization (i.e. Section 3.3.1), and the use of non-linear solvers was much more robust (i.e. we verified convergence even when increasing the number of modes taken into account). It is possible to employ commercial or open-source software to run these solvers (e.g. [53,54]). The procedure to manage these BMI problems is explained below and requires fixing some initial conditions. The case of H_∞ control coupled to the passivity constraint is considered here as an example for the sake of clarity (however, there are no differences for H_2 and mixed H_2 / H_∞ controls):

1. the order of the controller n_k is chosen (more details about such a choice will be provided at the end of the section) and a first-attempt real positive controller is fixed, finding the matrices $\mathbf{A}_{k,0}$, $\mathbf{B}_{k,0}$, $\mathbf{C}_{k,0}$, and $\mathbf{D}_{k,0}$. The subscript 0 indicates the first-attempt solution. Usually, we used the solution from the CF technique to fix the initial values of the matrices. Just the basic CF method was used [20] , without applying any optimisation [21,22];
2. once the matrices $\mathbf{A}_{k,0}$, $\mathbf{B}_{k,0}$, $\mathbf{C}_{k,0}$, and $\mathbf{D}_{k,0}$ are defined, they are used to solve both the linear H_∞ problem (Eq. (25)), finding the minimised γ and the related Lyapunov matrix $\mathbf{P}_\infty$, and the linear problem related to the passivity (Eq. (28)), which has the Lyapunov matrix $\mathbf{P}_k$ as the only unknown. It is noticed that, since the controller matrices are fixed to be equal to the first-attempt solution, both the H_∞ and the passivity problem are linear in the unknown variables γ and $\mathbf{P}_\infty$, and $\mathbf{P}_k$, respectively. The subscripts of the Lyapunov matrices are used to indicate the Lyapunov matrices related to the two different control problems. The resulting $\mathbf{P}$ matrices and γ value are referred to as $\mathbf{P}_{\infty,0}$, $\mathbf{P}_{k,0}$, and γ_0, since they are the first-attempt solutions;
3. then, the BMI solver uses $\mathbf{P}_{\infty,0}$, $\mathbf{P}_{k,0}$, γ_0, $\mathbf{A}_{k,0}$, $\mathbf{B}_{k,0}$, $\mathbf{C}_{k,0}$, and $\mathbf{D}_{k,0}$ as initial conditions for the multi-objective problem and minimises γ, providing $\mathbf{P}_{\infty,1}$, $\mathbf{P}_{k,1}$, γ_1, $\mathbf{A}_{k,1}$, $\mathbf{B}_{k,1}$, $\mathbf{C}_{k,1}$, and $\mathbf{D}_{k,1}$ as results. The problem formed by conditions (25) and (28) is a BMI because the unknowns are the Lyapunov matrices $\mathbf{P}_\infty$ and $\mathbf{P}_k$, as well as γ, $\mathbf{A}_k$, $\mathbf{B}_k$, $\mathbf{C}_k$, and $\mathbf{D}_k$;
4. step 3 is run again with $\mathbf{P}_{\infty,1}$, $\mathbf{P}_{k,1}$, γ_1, $\mathbf{A}_{k,1}$, $\mathbf{B}_{k,1}$, $\mathbf{C}_{k,1}$, and $\mathbf{D}_{k,1}$ as the initial conditions.

In this procedure, step 4 is then iterated until γ satisfies a certain stopping condition.

The procedure described allows to find $\mathbf{A}_k$, $\mathbf{B}_k$, $\mathbf{C}_k$, and $\mathbf{D}_k$ and thus the transfer function $K(s)$ of the controller. The transfer function of the impedance $Z(s)$ can then be calculated using Eq. (17). The order of the controller n_k must be chosen arbitrarily at the beginning of the procedure. We carried out different tests and found that the use of $n_k = n_s - 1$ and $n_k = n_s - 2$ provide good results. Nevertheless, n_k can be fixed to any desired value, keeping the method as general as possible. If n_k is kept lower

than n_s-2, the damping performance decreases, at least for part of the modes considered. If n_k is kept higher than n_s-1, no significant attenuation improvements are noticed, although the values of the required electrical components (e.g. inductances) can decrease if compared to the case of $n_k = n_s-1$. This allows for a simpler inductance implementation in certain applications, but it also leads to a higher complexity of the whole circuit because the number of elements constituting Z increases with n_k.

It is noticed that the non-linear solvers do not apply any linearization to the problem. The procedure used here requires only a linearization at the beginning to fix the initial conditions (item 2 in the previous list).

4. Synthesis of the shunt impedance

The order of the controller that results from the BMI problem is equal to n_k. As mentioned, this order is fixed by the user (see point 1 of the numbered list in Section 3.3.2) by imposing a first-attempt controller K_0 and then finding the corresponding first attempt matrices $\mathbf{A}_{k,0}$, $\mathbf{B}_{k,0}$, $\mathbf{C}_{k,0}$, and $\mathbf{D}_{k,0}$. These matrices thus have a fixed size, as do the matrices $\mathbf{A}_k$, $\mathbf{B}_k$, $\mathbf{C}_k$, and $\mathbf{D}_k$ resulting from the BMI problem. Hence, the resulting optimal controller K will have the same order n_k as in the first attempt. Its transfer function $K(s)$ has the following generic analytical form:

$$K(s) = \frac{\lambda_\sigma s^\sigma + \lambda_{\sigma-1} s^{\sigma-1} + \ldots + \lambda_1 s + \lambda_0}{\delta_\sigma s^\sigma + \delta_{\sigma-1} s^{\sigma-1} + \ldots + \delta_1 s + \delta_0} \tag{31}$$

The coefficients λ and δ are real positive scalars thanks to the passivity condition, and $\sigma = n_k$. According to Eq. (17), we have:

$$Z(s) = \frac{\delta_\sigma s^\sigma + \delta_{\sigma-1} s^{\sigma-1} + \ldots + \delta_1 s + \delta_0}{(\lambda_\sigma s^\sigma + \lambda_{\sigma-1} s^{\sigma-1} + \ldots + \lambda_1 s + \lambda_0) C_p} \tag{32}$$

This form of the impedance Z (i.e. real positive coefficients and equal orders of the numerator and denominator) guarantees practical realisability of the shunt circuit with passive elements (i.e. resistances, inductances, and capacitances) [55,56]. This is an important outcome of the BMI/LMI approach applied to the shunt damping.

There are a number of methods in the literature to synthetize an electric circuit starting from positive real transfer functions, and we used the classical method by Brune [57,58]. This method describes how to implement a finite one-port network where the driving-point impedance is a prescribed function. This approach enables the design of lumped-element equivalent circuits with a minimum number of elements, which are positive if the function describing the one-port impedance is positive real. The elements of the circuits are only capacitors, inductors, and resistors, and the interconnect structure generally contains ideal transformers [59]. No details about the method are given here for the sake of conciseness. However, details about the procedure are available elsewhere [57–59].

5. Experiments

This section describes the experimental tests carried out to show the effectiveness of the BMI/LMI approach to shunt damping. Section 5.1 describes the test setup, and Section 5.2 provides details about several tests where we simulated the shunt network using a synthetic impedance. Finally, Section 5.3 gives a detailed description of one of the tests carried out with a physically implemented shunt impedance Z.

5.1. Test setup

The experimental setup was an aluminium cantilever beam with one piezoelectric patch bonded at its clamped end. The beam was 161 mm long, 25 mm wide, and 1.1 mm thick, while the piezoelectric patch was 51 mm long, 25 mm wide, and 0.38 mm thick. The structure was excited by means of a contactless actuator composed of a coil and a magnet bonded to the beam near its tip (see Fig. 3a). Current flowing in the coil results in a proportional force exerted on the beam [60]. The current was measured using a current clamp, and the response of the structure was measured through a laser Doppler velocimeter in a co-located position with the exerted force (on the other side of the beam). The second, third, and fourth eigenmodes were considered, and their modal data are presented in Table 1. The eigenfrequencies and non-dimensional damping ratios were estimated by an experimental modal analysis with the piezoelectric patch short-circuited. The algorithm for modal parameter extraction was the polyreference least square frequency domain method. χ_r was estimated by means of measurements of the r^{th} coupling coefficient $k_r^{\text{eff}} = \sqrt{(\omega_{r,\text{oc}}^2 - \omega_r^2)/\omega_r^2}$ ($\omega_{r,\text{oc}}$ is the r^{th} eigenfrequency with the piezoelectric patch in open-circuit (OC)) and then making the following computation [6]:

$$\chi_r = k_r^{\text{eff}} \omega_r \sqrt{C_{\text{pr}}}. \tag{33}$$

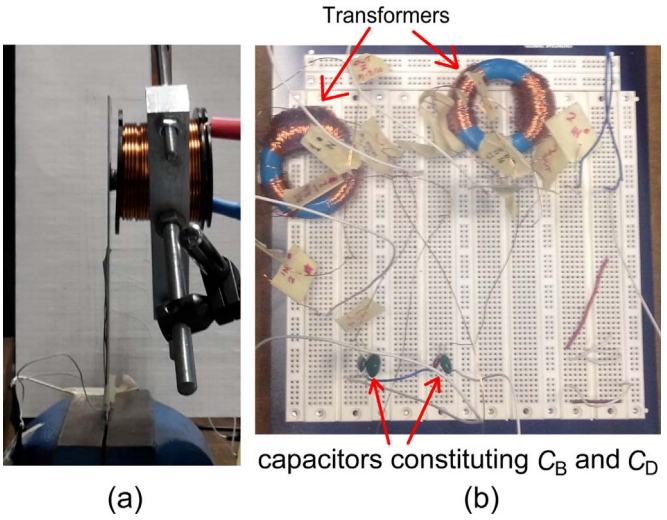

Fig. 3. Experimental setup (a) and the circuit used to implement the shunt impedance Z for H_2 control on the displacement of the third and fourth modes (see Section 5.3) (b). No resistances are visible in figure b, even if they were present in the circuit; indeed, they were made from the series of potentiometers for easy tuning and were not directly built on the board. The cables coming from these potentiometers and reaching the board are visible.

Table 1
Data of the experimental setup.

Mode number	$\omega_r/(2\pi)$ [Hz]	ξ_r [%]	k_r^{eff}
2	195.94	0.43	0.0428
3	500.98	0.40	0.0400
4	1004.39	0.44	0.0924

where C_{pr} is the measured piezoelectric capacitance value after the r^{th} eigenfrequency. The trend of the measured piezoelectric capacitance is plotted in Fig. 4. Fig. 5 shows the FRF of the system for the modes in Table 1.

The following subsections discuss the experiments. The reader will notice that the first mode is not used for these tests, where we considered H_∞, H_2, and mixed H_2 / H_∞ control. The reason is that the amplitude of the first mode in the transfer function T_{zF} is more than 10 dB higher than the amplitudes of the other three modes in short-circuit condition. This in turn means that the control action would basically be focused on just the first mode if it is taken into account when synthetizing the controller. This would prevent demonstration of the capabilities of the shunt impedance to work on many modes at the same time. Therefore, we aimed at damping the other three modes (modes 2, 3, and 4) in the tests shown herein.

5.2. *Tests with a synthetic impedance*

Many tests have been carried out to validate the BMI approach, but only some are described here for brevity. These tests were carried out without synthetizing a real passive shunt impedance (i.e. one made from resistances, capacitances, and inductances). Instead, a synthetic device was used to simulate the shunt impedance [61]. This approach allowed us to avoid any possible uncertainty about the values of the electric elements composing the shunt impedance and thus enabled to test the BMI approach without additional errors from external factors (i.e., uncertainty on the values of the electrical

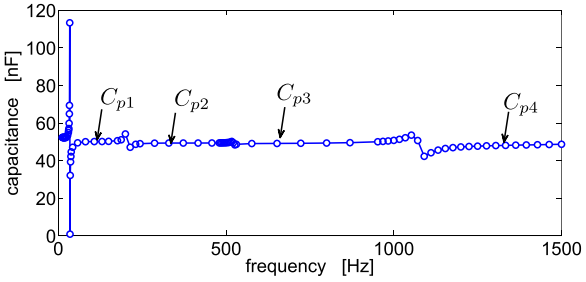

Fig. 4. Measured capacitance of the piezoelectric patch (circles are experimental measurements).

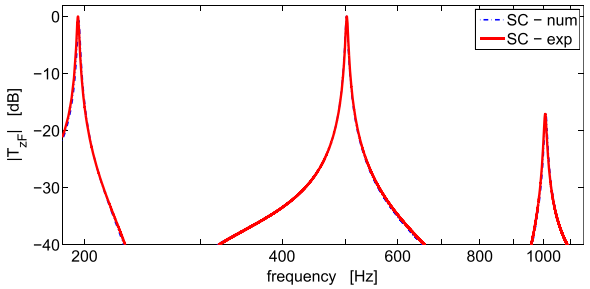

Fig. 5. Trend of $|T_{zF}|$ in SC. Experimental and numerical curves are almost superimposed.

parameters). Therefore, the use of the mentioned synthetic system was useful for testing the reliability of the LMI/BMI approach and was considered as the first step of the experiments.

Table 2 lists the tests considered and the attenuation levels achieved. Fig. 6 and Fig. 7 show comparisons between the numerical and experimental FRFs for tests A and B as examples. The value of n_k used to obtain these results was equal to twice the number of modes considered in the control problem, meaning that n_k was lower than the order of the EMS (i.e. $n_k = n_s - 1$). Table 2, Fig. 6 and Fig. 7 indicate good agreement between the numerical simulations and the experiments, thus demonstrating the effectiveness of the BMI approach and the reliability of the EMS model. Fig. 8 presents a magnification of the peaks in Fig. 7 for a clearer comparison of the curves.

One interesting result is related to the comparison between the attenuation provided by the BMI approach and those from well-established techniques using single piezoelectric actuators, CF and CB. Tests A and C from Table 2 are chosen as examples. Comparisons of the BMI results and those from the CB and CF methods are presented in Fig. 9a and Fig. 9b for test A and Fig. 9c and Fig. 9d for test C. In both cases, the CF technique fails to provide attenuation on the first considered mode (i.e. the CF and SC curves are almost superimposed for the first mode). This is mainly due to the difficulties associated with the minimisation procedure (see Section 1), which basically does not converge. The BMI instead always provides better results than the state-of-the-art methods. Such a result is really interesting, especially because the initial controller for the BMI approach is from the non-optimised CF method (see Section 3.3.2). Therefore, it is evident that the initial controller does not provide satisfactory results and that the BMI algorithm is then able to converge to a better solution successfully.

Fig. 9 thus highlights the reliability and the effectiveness of the BMI approach in finding the optimal controller for a given control problem. It is noticed that the CF and CB methods use either series or parallel resistances for each inductance. A more complex approach with a combination of series and parallel resistances for each inductance would make the damping performance closer to that of the BMI approach, but the choice of the values for these additional elements is not straightforward.

Finally, we applied the BMI method also for H_∞ control of just one mode (the results are not shown here for brevity). The optimal shunt impedance and the consequent attenuation for this kind of control on a single mode have already been described analytically in the literature [2]. BMI actually leads to this optimal solution, even when starting from an initial

Table 2
Description of tests with the order of the controller n_k equal to n_s-1.

Test ID	Target variable z_o	Test type	Attenuation (numerical) [dB]	Attenuation (experimental) [dB]	Difference (experiment–prediction) [dB]
A	Displacement	Mixed H_2/H_∞ on modes 3 and 4	11.0 on mode 3 11.9 on mode 4	10.5 on mode 3 12.1 on mode 4	-0.5 on mode 3 0.2 on mode 4
B	Displacement	Mixed H_2/H_∞ on modes 2, 3 and 4	6.9 on mode 2 5.0 on mode 3 15.2 on mode 4	6.5 on mode 2 4.9 on mode 3 14.6 on mode 4	-0.4 on mode 2 -0.1 on mode 3 -0.6 on mode 4
C	Displacement	H_∞ on modes 2 and 3	10.6 on mode 2 10.3 on mode 3	10.9 on mode 2 9.2 on mode 3	0.3 on mode 2 -1.1 on mode 3
D	Displacement	H_∞ on modes 3 and 4	12.2 on mode 3 7.0 on mode 4	11.6 on mode 3 6.7 on mode 4	-0.6 on mode 3 -0.3 on mode 4
E	Velocity	H_∞ on modes 2, 3 and 4	10.6 on mode 2 9.5 on mode 3 16.1 on mode 4	12.0 on mode 2 9.1 on mode 3 17.4 on mode 4	1.4 on mode 2 -0.4 on mode 3 1.3 on mode 4
F	Velocity	Mixed H_2/H_∞ on modes 3 and 4	3.1 on mode 3 14.3 on mode 4	3.0 on mode 3 14.1 on mode 4	-0.1 on mode 3 -0.2 on mode 4

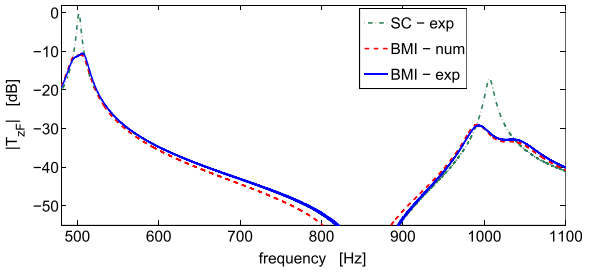

Fig. 6. Trend of $|T_{zF}|$ for test A.

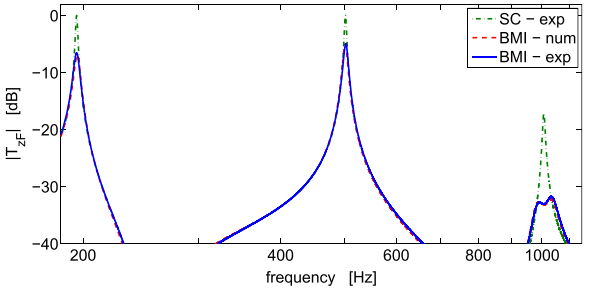

Fig. 7. Trend of $|T_{zF}|$ for test B.

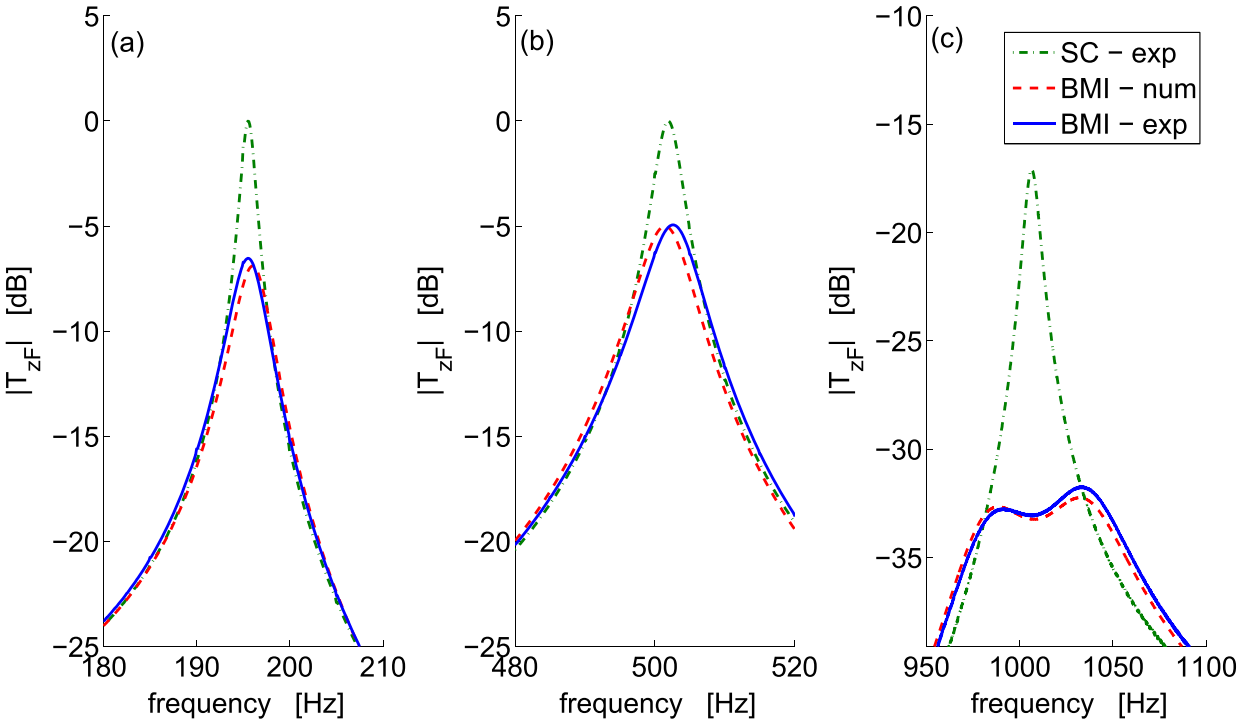

Fig. 8. Trend of $|T_{zF}|$ for test B; magnification of the peaks of Fig. 7: mode 2 (a), mode 3 (b), mode 4 (c).

controller (see Section 3.3.2) that is far from the optimal one (e.g. errors up to about 30% intentionally imposed on the electric components of the initial shunt impedance). In this case, even the linear solvers (see Section 3.3.1) can yield the optimal solution.

5.3. Test with practical implementation of the shunt impedance

The second step of the experiments involved using a real shunt impedance Z. We performed different tests and we discuss one of them in detail in this section, which is for H_2 control of the displacement of the third and fourth modes. The

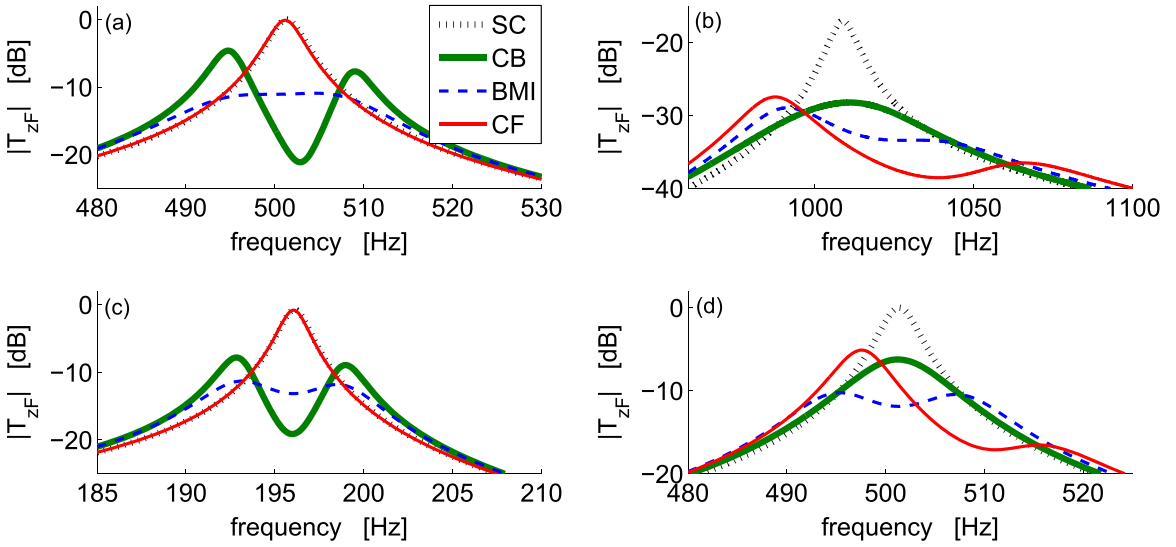

Fig. 9. Trend of $|T_{zF}|$: comparison of BMI, CF, and CB approaches (numerical results). Test A of Table 2, magnification of the third mode (a), test A, magnification of the fourth mode (b), test C, magnification of the second mode (c), test C, magnification of the third mode (d).

order n_k of the controller was set as n_s-1. The impedance Z resulting from the BMI problem had the following expression:

$$Z(s) = \frac{1.\,88\cdot10^{5}s^{4}+2.\,32\cdot10^{8}s^{3}+5.\,38\cdot10^{12}s^{2}+2.\,14\cdot10^{15}s+1.\,72\cdot10^{19}}{s^{4}+2.\,24\cdot10^{5}s^{3}+2.\,46\cdot10^{8}s^{2}+2.\,97\cdot10^{12}s+9.\,61\cdot10^{14}} \tag{34}$$

Brune's synthesis led to the network in Fig. 10 (see Table 3 for the values of the electric components). It is noticed that two negative inductances are present in the circuit (even though the whole shunt impedance is passive). These negative elements just come from Brune's synthesis procedure. This problem could be avoided by using other synthesis methods [55,56], but they may require higher complexity. Nevertheless, the whole shunt impedance is still passive, and such negative elements can be realised easily by using transformers (see Appendix C).

A critical aspect related to the practical implementation of the impedance in Fig. 10 is related the vertical branches (i.e. the wire with L_B and C_B and that with L_D and C_D), which should not have any resistance (see Fig. 10). However, the inductors and capacitors on these wires are not ideal and therefore show a resistance value that cannot be completely null. Nevertheless, this criticality can be reduced using some tricks when building the network. As an example, the capacitances can be implemented by small capacitances in parallel, resulting in a resistance value that is lower than that of a single capacitance. This makes these parasitic resistances small (in this case, $R_B = 0.07\ \Omega$ and $R_D = 0.92\ \Omega$) and thus unable to influence the behaviour of the shunt impedance.

Moreover, attention is needed when building all the resistances depicted in Fig. 10. Indeed R_A, R_C, and R_E must account for the resistance values associated with the non-ideal inductors in series with these resistors. Therefore, the optimal values of R_A, R_C and R_E were obtained by summing the residual resistance values of the non-ideal inductors with proper resistors in series. As an example, for a residual resistance $R_{A,L}$ of the inductor representing L_A, R_A has been obtained by adding a proper resistance R_x in series to the inductor such that $R_A = R_x + R_{A,L}$. The final layout of the shunt impedance is shown in Fig. 3b, which highlights the experimental setup used to build it.

The theoretical impedance (Fig. 10) matches well with the experimental results shown in Fig. 11. The experimental impedance was measured by imposing a voltage at the impedance terminals and measuring the current flowing in the

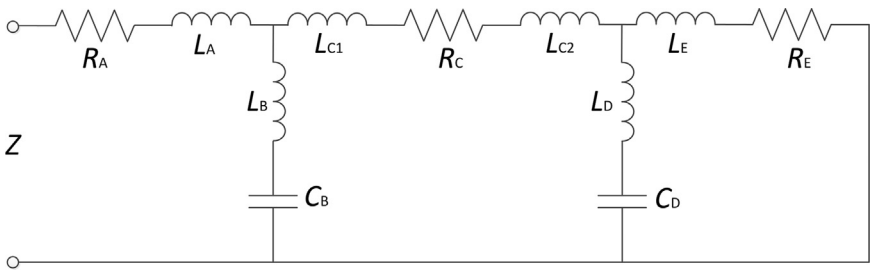

Fig. 10. Impedance Z (the values of the variables are provided in Table 3).

Table 3
Values of the parameters in Fig. 10.

R_A [Ω]	L_A [H]	C_B [μF]	L_B [mH]	R_C [Ω]	L_{C1} [mH]	L_{C2} [mH]	C_D [μF]	L_D [mH]	R_E [Ω]	L_E [mH]
89.64	1.31	35.84	80.7	1.98	-76.04	-0.27	5.43	7.8	330.5	0.28

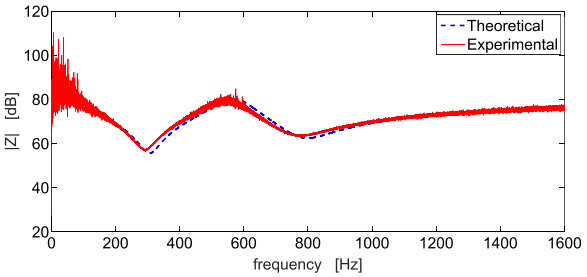

Fig. 11. Trend of |Z|: experimental and theoretical curves.

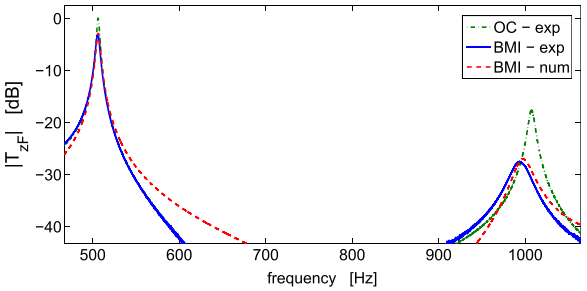

Fig. 12. Trend of $|T_{zF}|$: experimental and numerical curves (magnification of modes 3 and 4).

circuit. It is noticed that the shunt impedance provided by the BMI has a similar number of electric components to that provided by the CB when two modes are controlled (as in this case). However, the complexity of the CB shunt impedance increases much more than that of the BMI when the number of modes to be damped increases.

Fig. 12 shows the comparison between the experiments and the simulations in terms of $|T_{zF}|$. There is good agreement between the curves, showing the reliability of the model and the BMI approach, even in presence of a physical shunt network. The experimental FRFs were estimated using both chirp and random excitations, which produced similar results.

The capability of the BMI approach to provide satisfactory results paves the way for further development: the use of matrix inequalities not only to design the shunt impedance, but also to choose the number, type, and location of the actuators [62]. Indeed, the model described by Eqs. (4), (7), and (8), as well as its state space representation, can be extended to a case where more than one piezoelectric actuator is attached to the vibrating structure. This would allow for a global and general approach to shunt damping.

6. Conclusions

This paper has dealt with multi-modal vibration damping by means of shunted piezoelectric actuators. An approach based on matrix inequalities has been presented to provide good attenuation levels and assure the passivity and the realisability of the shunt impedance without posing restrictions on the impedance layout or requiring any arbitrary assumption on the network component values. This was made possible by setting up a multi-objective control problem based on matrix inequalities. The approach relies on the description of the electro-mechanical system using a state space representation where the shunt impedance is seen as a controller in a feedback loop.

The matrix inequality problem was shown to be non-linear; more specifically, a BMI problem. Thus, the solution requires non-obvious approaches. We tested two techniques: an iterative procedure based on the linearization of the problem using approximations (which enables the use of linear solvers), and non-linear solvers. These approaches allow for designing controllers with any desired order and pose no restrictions or conservatism on the solution. The use of non-linear solvers was more robust compared to the linearization of the problem using approximations.

The experiments showed that the proposed approach is reliable and effective. The BMI method achieved better attenuation performance than the well-established methods. This was also due to the possibility of posing specific control targets (e.g. H_2 and H_∞ control). The matrix inequality approach will be further investigated to the aim of developing of a general approach where the number, type, and location of actuators will also be considered as problem variables, as well as the features of the shunt impedance.

Appendix A

If the target of control is velocity reduction, we need to change the output variable z_o, which will no longer be displacement but velocity, i.e. $z_o = \dot{W}$. Therefore, we change the form of the matrix $\mathbf{C}_z$ (see Eq. (13)):

$$\mathbf{C}_z = \begin{bmatrix} \Phi_u(x_m) & 0 & \Phi_{u+1}(x_m) & 0 & \cdots & \Phi_h(x_m) & 0 & 0 \end{bmatrix} \tag{A.1}$$

For controlling acceleration, we need to change $\mathbf{C}_z$, $\mathbf{D}_{zw}$, and $\mathbf{D}_{zf}$ (see Eq. (13)):

$$\begin{aligned} &\mathbf{C}_z = \mathbf{C}_{zu} + \mathbf{C}_{z(u+1)} + \ldots + \mathbf{C}_{zh}; \mathbf{D}_{zf} = \Phi_u(x_m)\Phi_u(x_f) + \Phi_{u+1}(x_m)\Phi_{u+1}(x_f) + \ldots + \Phi_h(x_m)\Phi_h(x_f); \\ &\mathbf{D}_{zw} = \Phi_u(x_m)b_u\omega_u + \Phi_{u+1}(x_m)b_{u+1}\omega_{u+1} + \ldots + \Phi_h(x_m)b_h\omega_h \end{aligned} \tag{A.2}$$

where:

$$\mathbf{C}_{zu} = \Phi_u(x_m)\begin{bmatrix} -2\xi_u\omega_u & -\omega_u^2(1+b_u^2) & 0 & -\omega_u b_u \omega_{u+1} b_{u+1} & \cdots & 0 & -\omega_u b_u \omega_h b_h & -\dfrac{b_u\omega_u}{R_p C_p} \end{bmatrix} \tag{A.3}$$

$$\mathbf{C}_{z(u+1)} = \Phi_{u+1}(x_m)\begin{bmatrix} 0 & -\omega_{u+1} b_{u+1} \omega_u b_u & -2\xi_{u+1}\omega_{u+1} & -\omega_{u+1}^2\left(1+b_{u+1}^2\right) & \cdots & 0 & -\omega_{u+1} b_{u+1} \omega_h b_h & -\dfrac{b_{u+1}\omega_{u+1}}{R_p C_p} \end{bmatrix} \tag{A.4}$$

$$\mathbf{C}_{zh} = \Phi_h(x_m)\begin{bmatrix} 0 & -\omega_h b_h \omega_u b_u & 0 & -\omega_h b_h \omega_{u+1} b_{u+1} & \cdots & -2\xi_h\omega_h & -\omega_h^2\left(1+b_h^2\right) & -\dfrac{b_h\omega_h}{R_p C_p} \end{bmatrix} \tag{A.5}$$

Appendix B

The expressions of matrices $\mathbf{A}_{cl}$, $\mathbf{B}_{cl}$, $\mathbf{C}_{cl}$, and $\mathbf{D}_{cl}$ (see Eq. (21)) for $z_o = W$, $z_o = \dot{W}$, and $z_o = \ddot{W}$ are as follows:

$$\mathbf{A}_{cl} = \begin{bmatrix} \mathbf{A} + \boldsymbol{B}_w\mathbf{D}_k\mathbf{C}_y & \boldsymbol{B}_w\mathbf{C}_k \\ \boldsymbol{B}_k\mathbf{C}_y & \mathbf{A}_k \end{bmatrix}, \mathbf{B}_{cl} = \begin{bmatrix} \mathbf{B}_f \\ \mathbf{0} \end{bmatrix}, \mathbf{C}_{cl} = \begin{bmatrix} \mathbf{C}_z + \mathbf{D}_{zw}\mathbf{D}_k\mathbf{C}_y & \mathbf{D}_{zw}\mathbf{C}_k \end{bmatrix}, \mathbf{D}_{cl} = \begin{bmatrix} \mathbf{D}_{zf} \end{bmatrix} \tag{B.1}$$

Appendix C

When Brune's method is used to synthesise the electrical network, the possible presence of negative inductances in the circuit is always associated with the configuration shown in Fig. C.1a, where L_1 and L_2 are positive inductances, while L_3 is a negative one. Such a circuit can be practically implemented relying on the transformer concept, based on inductances L_p and L_s (see Fig. C.1b). Indeed, the use of the transformer allows us to reproduce the behaviour of the circuit in Fig. C.1a according to the following equations:

$$\begin{cases} L_1 = L_p + k_{trasf}\sqrt{L_p L_s} \\ L_2 = L_s + k_{trasf}\sqrt{L_p L_s} \\ L_3 = -k_{trasf}\sqrt{L_p L_s} \end{cases} \tag{C.1}$$

where $0 \le k_{trasf} \le 1$; k_{trasf} is the coupling coefficient of the transformer, which expresses its efficiency.
According to Eq. (C.1), it is thus possible to derive the values of L_p, L_s, and k_{trasf} from the desired values of L_1, L_2, and L_3:

$$\begin{cases} L_p = L_1 + L_3 \\ L_s = L_2 + L_3 \\ k_{trasf} = -\dfrac{L_3}{\sqrt{L_p L_s}} \end{cases} \tag{C.2}$$

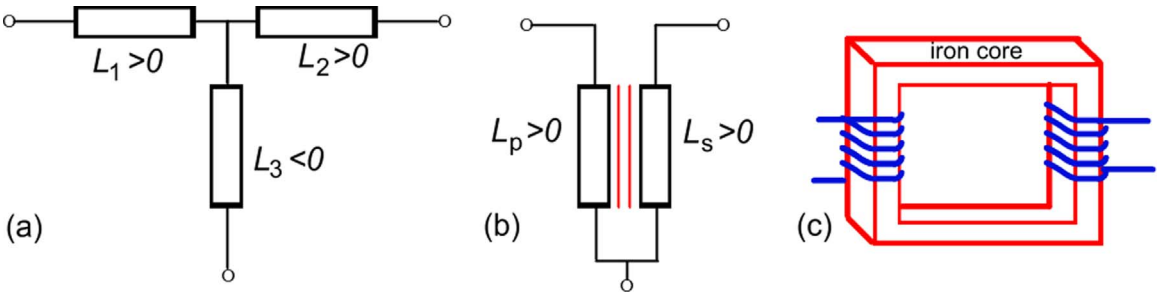

Fig. C.1. Circuit to build (a), its practical realisation (b), and the layout of the transformer (c).

It is possible to demonstrate that when Brune's method leads to the network in Fig. C.1a, the value of k_{trasf} is equal to 1 (i.e. perfect coupling) [57]. A practical implementation of the transformer in Fig. C.1b is shown in Fig. C.1c. The values of L_p and L_s depend on the relative magnetic permeability μ_m, the area A_s crossed by the flux, and the mean path of the flux lines l_f:

$$\begin{cases} L_p = N_{cp}^2 \left(P_{11} + \dfrac{\mu_m A_s}{l_f} \right) \\ L_s = N_{cs}^2 \left(P_{22} + \dfrac{\mu_m A_s}{l_f} \right) \end{cases} \tag{C.3}$$

where N_{cp} and N_{cs} are the numbers of turns of the coils of L_p and L_s, respectively. P_{11} and P_{22} are the dispersions of the transformer due to non-perfect coupling (P_{11} and P_{22} must be null in this case because $k_{trasf} = 1$). In this application, the transformer was built with an iron ring as a core, with an inner diameter of 28.5 mm, outer diameter of 51.8 mm, and thickness of 21.3 mm. Finally, μ_m was 4300.

Even if the perfect coupling required by Brune's method is not physically feasible, a value of k_{trasf} near 1 can be achieved with the typical values of the electrical variables involved in shunt applications and properly designing and building the circuit. This can be seen in the experimental FRF of the shunt impedance used in this application in Fig. 11. This experimental FRF matches well the theoretical one, which means that the value of k_{trasf} is sufficiently near 1. More details about transformers can be found in the wide referenced literature (e.g. [63]).

References

[1] N. Hagood, A. von Flotow, Damping of structural vibrations with piezoelectric materials and passive electrical networks, J. Sound Vib. 146 (1991) 243–268.
[2] O. Thomas, J. Ducarne, J.-F. Deü, Performance of piezoelectric shunts for vibration reduction, Smart Mater. Struct. 21 (2012) 15008, http://dx.doi.org/10.1088/0964-1726/21/1/015008.
[3] K. Yamada, H. Matsuhisa, H. Utsuno, K. Sawada, Optimum tuning of series and parallel LR circuits for passive vibration suppression using piezoelectric elements, J. Sound Vib. 329 (2010) 5036–5057, http://dx.doi.org/10.1016/j.jsv.2010.06.021.
[4] M. Berardengo, A. Cigada, S. Manzoni, M. Vanali, Vibration control by means of piezoelectric actuators shunted with LR impedances: performance and robustness analysis, Shock and Vibration., (2015), http://dx.doi.org/10.1155/2015/704265. Paper ID:704265.
[5] M. Berardengo, S. Manzoni, M. Vanali, The behaviour of mistuned piezoelectric shunt systems and its estimation, Shock Vib. 2016 (2016) 9739217, http://dx.doi.org/10.1155/2016/9739217.
[6] M. Berardengo, O. Thomas, C. Giraud-Audine, S. Manzoni, Improved resistive shunt by means of negative capacitance: new circuit, performances and multi-mode control, Smart Mater. Struct. 25 (2016) 75033, http://dx.doi.org/10.1088/0964-1726/25/7/075033.
[7] B. de Marneffe, A. Preumont, Vibration damping with negative capacitance shunts: theory and experiment, Smart Mater. Struct. 17 (2008) 35015, http://dx.doi.org/10.1088/0964-1726/17/3/035015.
[8] C.H. Park, A. Baz, Vibration control of beams with negative capacitive shunting of interdigital electrode piezoceramics, J. Vib. Control. 11 (2005) 331–346, http://dx.doi.org/10.1177/107754605040949.
[9] M. Berardengo, O. Thomas, C. Giraud-Audine, S. Manzoni, Improved shunt damping with two negative capacitances: an efficient alternative to resonant shunt, J. Intell. Mater. Syst. Struct. http://dx.doi.org/10.1177/1045389X16667556.
[10] M. Neubauer, R. Oleskiewicz, K. Popp, T. Krzyzynski, Optimization of damping and absorbing performance of shunted piezo elements utilizing negative capacitance, J. Sound Vib. 298 (2006) 84–107, http://dx.doi.org/10.1016/j.jsv.2006.04.043.
[11] B.S. Beck, K. a Cunefare, M. Collet, The power output and efficiency of a negative capacitance shunt for vibration control of a flexural system, Smart, Mater. Struct. 22 (2013) 65009, http://dx.doi.org/10.1088/0964-1726/22/6/065009.
[12] M. Berardengo, S. Manzoni, O. Thomas, C. Giraud-Audine, A new electrical circuit with negative capacitances to enhance resistive shunt damping, in: Proceedings of the ASME 2015 Conference on Smart Materials, Adaptive Structures and Intelligent Systems - SMASIS 2015 - September 21-23 2015, Colorado Springs (CO, USA), 2015: p. ID 8836.
[13] M. Pohl, Increasing the performance of negative capacitance shunts by enlarging the output voltage to the requirements of piezoelectric transducers, J. Intell. Mater. Syst. Struct. http://dx.doi.org/10.1177/1045389X16666181.
[14] S. Behrens, A.J. Fleming, S.O.R. Moheimani, A broadband controller for shunt piezoelectric damping of structural vibration, Smart Mater. Struct. 18 (2003) 18–28.
[15] D. Guyomar, A. Badel, Nonlinear semi-passive multimodal vibration damping: an efficient probabilistic approach, J. Sound Vib. 294 (2006) 249–268, http://dx.doi.org/10.1016/j.jsv.2005.11.010.

[16] A. Badel, G. Sebald, D. Guyomar, M. Lallart, E. Lefeuvre, C. Richard, et al., Piezoelectric vibration control by synchronized switching on adaptive voltage sources: towards wideband semi-active damping, J. Acoust. Soc. Am. 119 (2006) 2815–2825.
[17] M. Lallart, É. Lefeuvre, C. Richard, D. Guyomar, Self-powered circuit for broadband, multimodal piezoelectric vibration control, Sens. Actuators A: Phys. 143 (2008) 377–382, http://dx.doi.org/10.1016/j.sna.2007.11.017.
[18] J.J. Hollkamp, Multimodal passive vibration suppression with piezoelectric materials and resonant shunts, J. Intell. Mater. Syst. Struct. 5 (1994) 49–57.
[19] S. Wu, Method for multiple-mode shunt damping of structural vibration using a single PZT transducer, in: Proceedings SPIE 3327, Smart Structures and Materials 1998: Passive Damping and Isolation, San Diego (USA), 1998.
[20] S. Behrens, S.O.R. Moheimani, a J. Fleming, Multiple mode current flowing passive piezoelectric shunt controller, J. Sound Vib. 266 (2003) 929–942, http://dx.doi.org/10.1016/S0022-460X(02)01380-9.
[21] S. Behrens, S.O.R. Moheimani, Optimal resistive elements for multiple mode shunt damping of a piezoelectric laminate beam, in: Proceedings of the 39th IEEE Conference on Decision and Control, Sydney, 2000.
[22] A. Cigada, S. Manzoni, M. Redaelli, M. Vanali, Optimization of the current flowing technique aimed at semi-passive multi-modal vibration reduction, J. Vib. Control. 18 (2012) 298–312, http://dx.doi.org/10.1177/1077546311407537.
[23] A.J. Fleming, S. Behrens, S.O.R. Moheimani, Reducing the inductance requirements of piezoelectric shunt damping systems, Smart Mater. Struct. 12 (2003) 57–64, http://dx.doi.org/10.1088/0964-1726/12/1/307.
[24] I. Giorgio, Multimode collocated vibration control with multiple piezoelectric transducers (PhD Thesis), Università degli Studi di Roma “La Sapienza,”, 2008.
[25] S. Moheimani, A. Fleming, S. Behrens, Dynamics, stability, and control of multivariable piezoelectric shunts, ASME Trans. 9 (2004) 87–99, http://dx.doi.org/10.1109/TMECH.2004.823882.
[26] A.J. Fleming, S.O.R. Moheimani, Control orientated synthesis of high-performance piezoelectric shunt impedances for structural vibration control, IEEE Trans. Control Syst. Technol. 13 (2005) 98–112, http://dx.doi.org/10.1109/TCST.2004.838547.
[27] C. Maurini, F. Dell'Isola, D. Del Vescovo, Comparison of piezoelectronic networks acting as distributed vibration absorbers, Mech. Syst. Signal Process. 18 (2004) 1243–1271, http://dx.doi.org/10.1016/S0888-3270(03)00082-7.
[28] R.C. Batra, F. Dell'Isola, S. Vidoli, D. Vigilante, Multimode vibration suppression with passive two-terminal distributed network incorporating piezoceramic transducers, Int. J. Solids Struct. 42 (2005) 3115–3132, http://dx.doi.org/10.1016/j.ijsolstr.2004.11.004.
[29] I. Giorgio, A. Culla, D. Del Vescovo, Multimode vibration control using several piezoelectric transducers shunted with a multiterminal network, Arch. Appl. Mech. 79 (2009) 859–879, http://dx.doi.org/10.1007/s00419-008-0258-x.
[30] U. Andreaus, F. Dell'Isola, M. Porfiri, Piezoelectric passive distributed controllers for beam flexural vibrations, J. Vib. Control 10 (2004) 625–659, http://dx.doi.org/10.1017/CBO9781107415324.004.
[31] P. Bisegna, G. Caruso, F. Maceri, Optimized electric networks for vibration damping of piezoactuated beams, J. Sound Vib. 289 (2006) 908–937, http://dx.doi.org/10.1016/j.jsv.2005.02.045.
[32] B. Lossouarn, J.-F. Deü, M. Aucejo, Multimodal vibration damping of a beam with a periodic array of piezoelectric patches connected to a passive electrical network, Smart Mater. Struct. 24 (2015) 1–14, http://dx.doi.org/10.1117/12.2083835.
[33] B. Lossouarn, J. Deü, M. Aucejo, K.A. Cunefare, Multimodal vibration damping of a plate by piezoelectric coupling to its analogous electrical network, Smart Mater. Struct. 25 (2016) 115042, http://dx.doi.org/10.1088/0964-1726/25/11/115042.
[34] L. Airoldi, M. Ruzzene, Wave propagation control in beams through periodic multi-branch shunts, J. Intell. Mater. Syst. Struct. 22 (2011) 1567–1579, http://dx.doi.org/10.1177/1045389X11408372.
[35] M. Collet, M. Ouisse, M.N. Ichchou, Structural energy flow optimization through adaptive shunted piezoelectric metacomposites, J. Intell. Mater. Syst. Struct. 23 (2012) 1661–1677, http://dx.doi.org/10.1177/1045389X12449915.
[36] B. Bao, D. Guyomar, M. Lallart, Vibration reduction for smart periodic structures via periodic piezoelectric arrays with nonlinear interleaved-switched electronic networks, Mech. Syst. Signal Process. 82 (2017) 230–259, http://dx.doi.org/10.1016/j.ymssp.2016.05.021.
[37] L. Yan, B. Bao, D. Guyomar, M. Lallart, Periodic structure with interconnected nonlinear electrical networks, J. Intell. Mater. Syst. Struct. 28 (2017) 204–229, http://dx.doi.org/10.1177/1045389X16649448.
[38] O. Thomas, J. Deü, J. Ducarne, Vibrations of an elastic structure with shunted piezoelectric patches: efficient finite element formulation and electromechanical coupling coefficients, Int. J. Numer. Methods Eng. 80 (2009) 235–268, http://dx.doi.org/10.1002/nme.
[39] J. Ducarne, O. Thomas, J.-F. Deü, Placement and dimension optimization of shunted piezoelectric patches for vibration reduction, J. Sound Vib. 331 (2012) 3286–3303, http://dx.doi.org/10.1016/j.jsv.2012.03.002.
[40] E. Doebelin, Measurement Systems: Application and Design, McGraw-Hill, New York, 2003.
[41] R. Skelton, T. Iwasaki, D. Grigoriadis, A Unified Algebraic Approach to Control Design, Taylor and Francis, London, 1998.
[42] G.-R. Duan, H.-H. Yu, LMIs in Control Systems - Analysis, Design and Applications, Press, CRC, Boca Raton (FL, USA), 2013.
[43] C. Scherer, P. Gahinet, M. Chilali, Multiobjective output-feedback, IEEE Trans. Autom. Control. 42 (1997) 896–911.
[44] S. Boyd, L. El Ghaoui, E. Feron, BalakrishnanV, Linear Matrix Inequalities in System and Control Theory, Society for Industrial and Applied Mathematics, 1994.
[45] C. Papageorgiou, M. Smith, Positive real synthesis using matrix inequalities for mechanical networks: application to vehicle suspension, IEEE Trans. Control Syst. Technol. 14 (2006) 423–435.
[46] F.A. Potra, S.J. Wright, Interior-point methods, J. Comput. Appl. Math. 124 (2000) 281–302, http://dx.doi.org/10.1016/S0377-0427(00)00433-7.
[47] A. Hassibi, J. How, S. Boyd, A path-following method for solving BMI problems in control, in: Proceedings of the 1999 American Control Conference, June 2-4 1999, San Diego (USA)pp. 1385–1389. doi:http://dx.doi.org/10.1109/ACC.1999.783595, 1999.
[48] J. Loftberg, YALMIP : A Toolbox for Modeling and Optimization in MATLAB, in: CACSD Conference, Taipei, Taiwan, 2004.
[49] YALMIP, Web Page. ⟨https://yalmip.github.io/⟩.
[50] MOSEK ApS, Web Page. ⟨https://www.mosek.com/⟩.
[51] M. Stingl, On the solution of nonlinear semidefinite programs by augmented Lagrangian methods (PhD thesis), University of Erlangen-Nurnberg, 2006.
[52] A. Conn, N. Gould, P. Toint, Trust Region methods, Society for Industrial and Applied Mathematics, 2000.
[53] PENOPT solvers, Web Page. ⟨http://www.penopt.com/⟩.
[54] TOMLAB/PENBMI, Web Page. ⟨http://tomopt.com/tomlab/products/penbmi/⟩.
[55] H. Baher, Synthesis of Electrical Network, Wiley, New York, 1984.
[56] F. Kuo, Network Analysis and Synthesis, 2nd ed, Wiley, 1966.
[57] O. Brune, Synthesis of a finite two-terminal network whose driving-point impedance is a prescribed function of frequency, J. Math. Phys. 10 (1931) 191–236.
[58] E.A. Guillemin, Synthesis of Passive Networks, John Wiley & Sons, New York, 1957.
[59] F. Mukhtar, Y. Kuznetsov, P. Russer, Network modelling with Brune's synthesis, Adv. Radio Sci. 9 (2011) 91–94, http://dx.doi.org/10.5194/ars-9-91-2011.
[60] O. Thomas, C. Touzé, a Chaigne, Asymmetric non-linear forced vibrations of free-edge circular plates. Part II: experiments, J. Sound Vib. 265 (2003) 1075–1101, http://dx.doi.org/10.1016/S0022-460X(02)01564-X.
[61] S. Moheimani, A. Fleming, Piezoelectric Transducers for Vibration Control and Damping, Springer, London, 2006.
[62] F. Li, M. de Oliveira, R. Skelton, Integrating information architecture and control or estimation design, SICE J. Control Meas. Syst. Integr. 1 (2011) 120–128.
[63] W. Hurley, D. Wilcox, Calculation of leakage inductance in transformers windings, IEEE Trans. Power Electron. 9 (1994) 121–126.